Electronic Supplementary Material (ESI) for Journal of Materials Chemistry A.

Photoelectrochemical Reduction of N_2 to NH_3 under Ambient Conditions through Hierarchical $MoSe_2$@*g*-C_3N_4 Heterojunctions

Muhammad Asim Mushtaq,[ab] Muhammad Arif,[ab] Xiaoyu Fang,[b] Ghulam Yasin,[a] Wen Ye,[b] Majid Basharat,[a] Bo Zhou,[b] Shiyu Yang,[b] Shengfu Ji,*[a] and Dongpeng Yan*[ab]

[a]State Key Laboratory of Chemical Resource Engineering, Beijing University of Chemical Technology, Beijing 100029, People's Republic of China.

[b]Beijing Key Laboratory of Energy Conversion and Storage Materials, College of Chemistry, Beijing Normal University, Beijing 100875, People's Republic of China.

*Corresponding authors:

Dongpeng Yan

Email: yandp@bnu.edu.cn

Shengfu Ji

Email: jisf@mail.buct.edu.cn

1. Photoelectrochemical measurements

All PEC measurements were performed at ambient conditions on CHI 760E electrochemical workstation with a gas-tight two-compartment H-type cell separated through a Nafion 211 membrane. Prior to use, the membrane was treated in 5% H_2O_2 and 0.5 M H_2SO_4 aqueous solution, followed by DI water at 80 °C for 1 h and finally rinsed with DI water. For future use, all membranes were immersed in DI water. Pt mesh (1×1 cm^2) was utilized as a counter electrode while Ag/AgCl/sat. KCl was performed as a reference electrode. All measured potential was calibrated to the reversible hydrogen electrode (RHE) by Nernst equation ($E_{RHE} = E_{Ag/AgCl} + 0.197 + 0.059$ pH). Xenon (Xe) arc lamp of 300 W from Newport Corporation tailored with an air mass (AM) 1.5 G filter was used for light illumination. The power density of the Xe arc lamp was corrected as 100 mW cm^{-2} and calibrated. All photoelectrocatalytic NRR assays were performed in 100 mL N_2 pre-saturated electrolytes, moreover pure N_2 consistently fed into the cathodic chamber of the cell. All applied potential were iR-compensated and geometric surface areas were obtained from current density values.

The average lifetime of the photogenerated electron-hole pairs calculated according to the following equation from the OCVD measurement (Equation 1).[1]

$$\tau_n = -\frac{K_B T}{q}\left(\frac{dV_{\propto}}{dt}\right)^{-1} \qquad (1)$$

where *"τ_n"* is the average lifetime of the photogenerated electron-hole pairs, *"K_B"* is the Boltzmann constant, *"T"* is the temperature (in Kelvin), *"q"* is the elementary charge of an electron and "$V_{\propto}$" is the open-circuit voltage.

2. Determination of NH_3

The NH_3 concentration was quantitatively calculated by the indophenol blue method via UV–vis spectrophotometry. Firstly, 2 mL electrolyte was pipetted from the cathodic chamber after electrolysis of gaseous N_2 and added into 2 mL of 1 M NaOH solution carry $C_7H_6O_3$ (5 wt%) and $Na_3C_6H_5O_7$ (5 wt%); furthermore, 1 mL of 0.05 M NaClO solution and 0.2 mL of $C_5FeN_6Na_2O{\cdot}2H_2O$ (1 wt%) coloring solution were added. Aliquots of electrolytes stained by indophenol blue and incubated for 2 h before UV–vis spectrophotometric measurements. For quantification of synthesized NH_3, a range of standard NH_4Cl solutions was utilized to established calibration curves. Background absorbance spectra of reference solutions (pure electrolytes) were also acquired to nullify the effects of electrolyte.

3. Detection of hydrazine

Watt and Chrisp's method was used to determine the traces of hydrazine (N_2H_4) that exist in 0.1 M KOH electrolyte after electrolysis. A mixture of p-$C_9H_{11}NO$ (5.99 g), HCI (concentrated, 30 mL), and C_2H_5OH (300 mL) was utilized as a color reagent. Series of 5 mL N_2H_4 standard solutions of concentrations 0.0, 0.3, 0.5, 0.7, 0.9, and 1.0 μg mL^{-1} in 0.1 M HCl were made to construct calibration curve. Afterward, for each concentration 5 mL of N_2H_4 standard solution was mixed with the 5 mL of the aforementioned color solution and stirred vigorously for 10 min at environmental temperature. The absorbance intensity of the resultant solutions was evaluated carefully at 455 nm, and N_2H_4 yields were predicted with the standard calibration curve. A satisfactory linear connection of absorbance with $N_2H_4{\cdot}H_2O$ concentration was observed from the calibration curve (Figure S23a).

4. Determination of NH_3 yield rate and Faradaic efficiency

NH_3 yield rate was estimated through the subsequent equation:

$$\text{Yield rate} = (C_{NH_3} \times V)/(t \times A) \quad (2)$$

where $"C_{NH_3}"$ is the concentration of produced NH_3, *"V"* refers to electrolyte volume, "*t*" is the reaction time and "*A*" stands for the working electrode surface area. Considering that three electrons take part to create one NH_3 molecule, the Faradaic efficiency was determined by the equation as follow:

$$\text{Faradaic efficiency} = (3F \times C_{NH_3} \times V)/17 * Q \quad (3)$$

where "F" is the Faraday constant and "Q" represents the total charge pass through the electrode during N_2 reduction reaction.

5. $^{15}N_2$ isotope labeling experiments

For the $^{15}N_2$ isotopic labeling, the electrolyte was deaerated by Ar gas for 30 min. Later, feeding gas $^{15}N_2$ was provided into the cathodic chamber for photoelectrolysis at −0.3 V vs. RHE. After 6 h of electrolysis, the electrolyte was collected and kept pH = 7 with 0.5 M H_2SO_4 solution, which was further concentrated through vacuum distillation. After being dissolved in D_2O, the sample was subjected to ^{1}H nuclear magnetic resonance (^{1}H NMR) analysis.

6. Computational analysis

All computations were performed in the Vienna ab initio simulation package (VASP) within the framework of the density functional theory (DFT) and the projector augmented plane-wave approach.[2] Generalized gradient approximation is chosen for the exchange-correlation potential.[3] The DFT-D3 technique is used to describe the long-range van der Waals interaction.[4] The plane wave energy cut-off is fixed at 400 eV. In the iterative solution of the Kohn-Sham equation, the energy constraint is established at 10^{-5} eV. Integration of the Brillouin zone attained at the Gamma point. All the structures are relaxed till the residual forces on the atoms decayed to <0.05 eV $Å^{-1}$. For all NRR, the Gibbs free energy (ΔG) was described as follows.[5]

$$\Delta G = \Delta E + \Delta E_{ZPE} - T\Delta S \quad (4)$$

where, "ΔE" denoted the energy of adsorption, "ΔE_{ZPE}" represent the zero-point energy changes, T=298.15 K (room temperature), and "ΔS" is the variations in entropy.

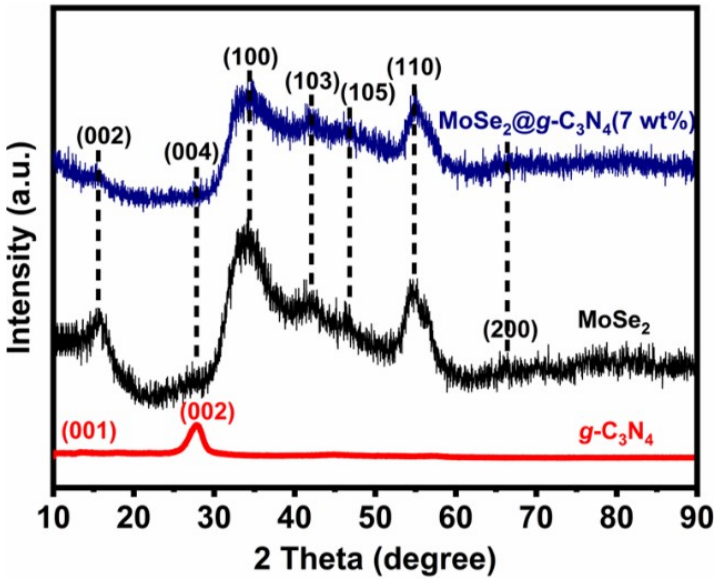

Figure S1: XRD pattern of g-C_3N_4, $MoSe_2$ and $MoSe_2$@g-C_3N_4 (7 wt%) hybrid.

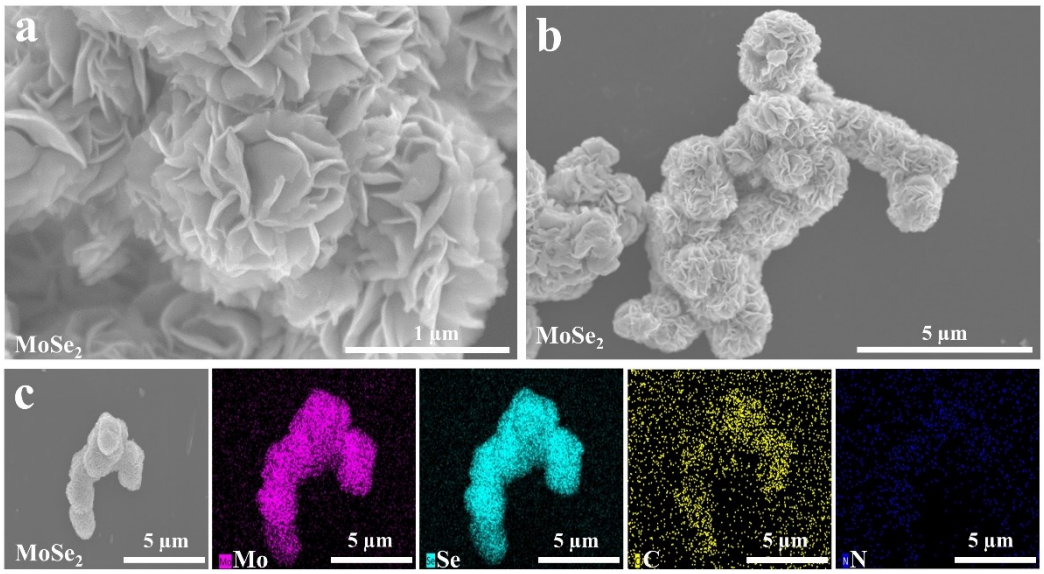

Figure S2: SEM images (a and b) $MoSe_2$, (c) EDS mapping of $MoSe_2$.

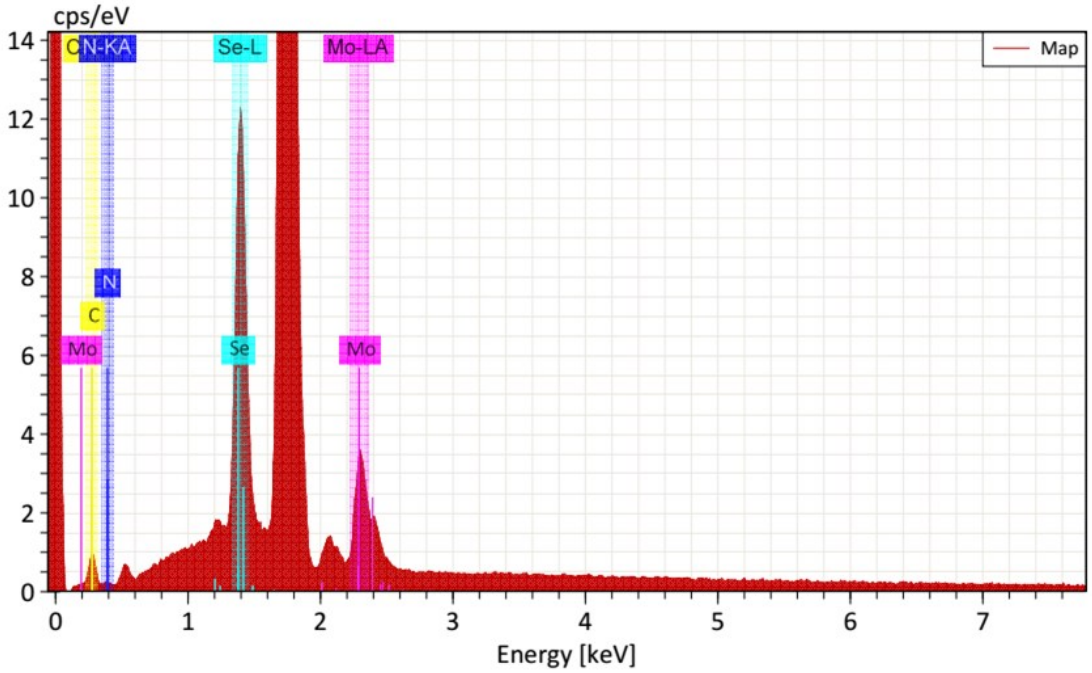

Figure S3: EDS spectrum of $MoSe_2$.

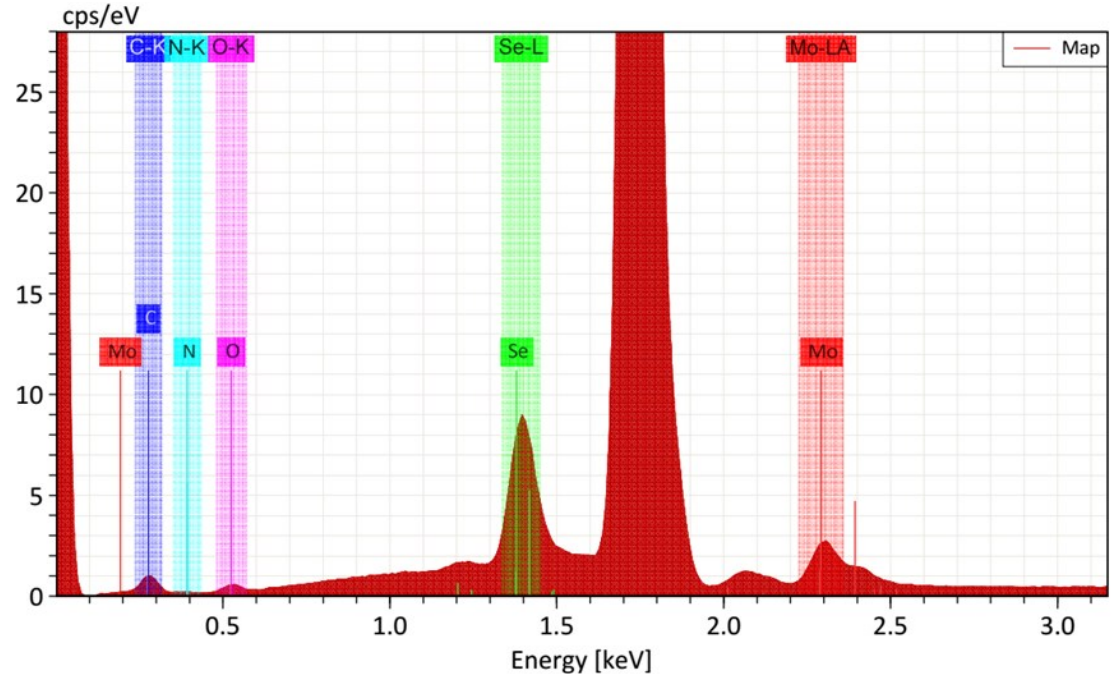

Figure S4: EDS spectrum of $MoSe_2$@*g*-C_3N_4 (7 wt%) hybrid.

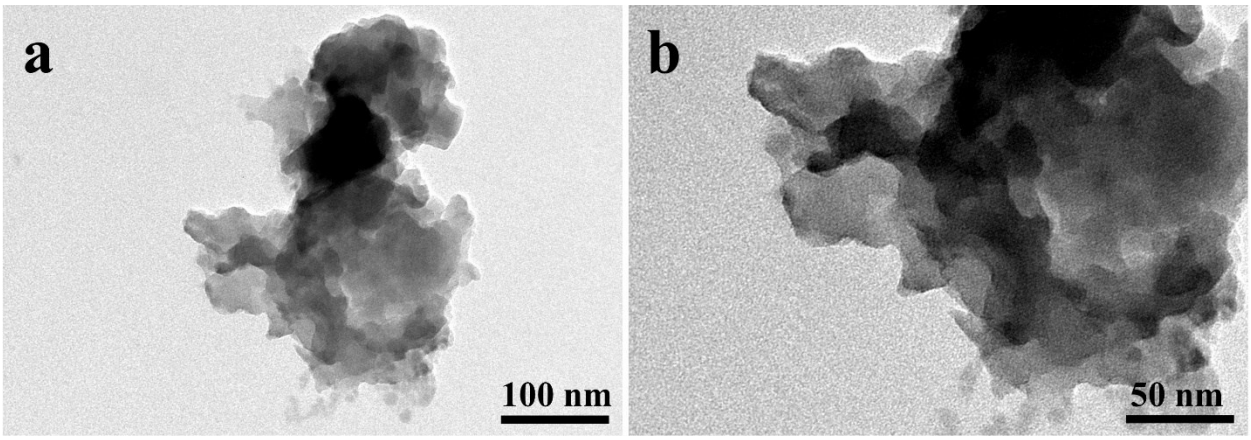

Figure S5: TEM images of pure *g*-C_3N_4 nanosheets.

Table S1: The average fluorescence lifetimes of *g*-C_3N_4 and $MoSe_2$@*g*-C_3N_4 (7 wt%).

Samples	**Lifetime τ** ns	**Pre-exponential factors *B***	**Average lifetime τ** ns
g-C_3N_4	τ_1=0.44	B_1=95.28	2.548
	τ_2=5.78	B_2=4.72	
$MoSe_2$@*g*-C_3N_4 (7 wt%)	τ_1=1.45	B_1=52.98	11.001
	τ_2=6.70	B_2=32.64	
	τ_3=34.50	B_3=14.38	

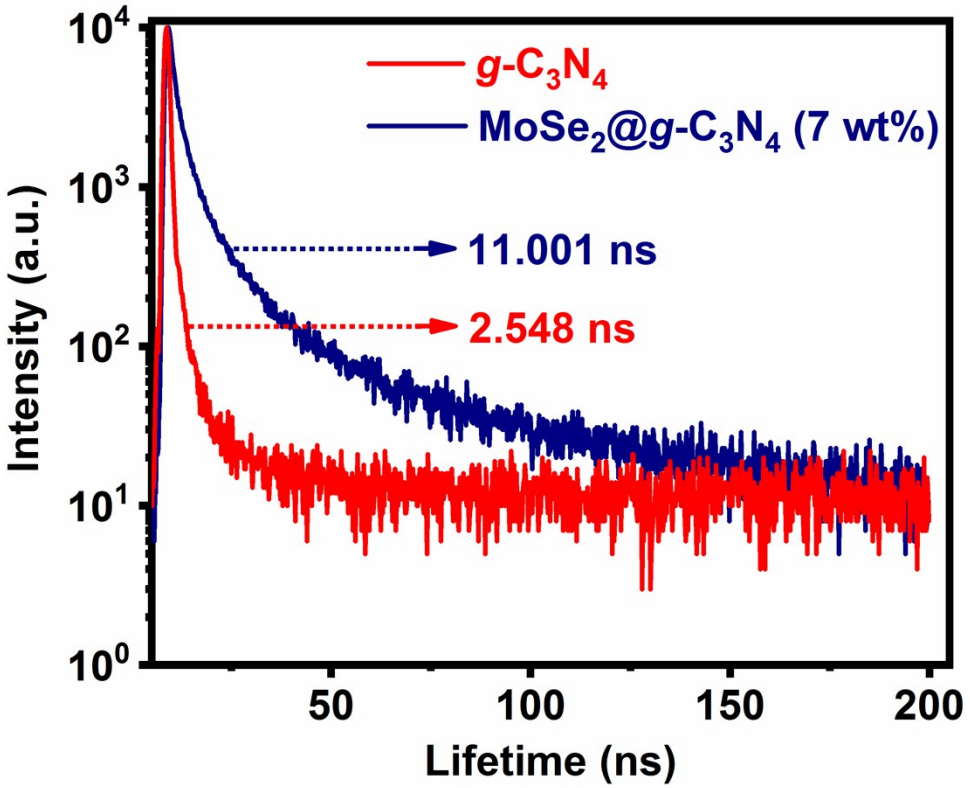

Figure S6: Fluorescence lifetime spectra of g-C_3N_4 and $MoSe_2$@g-C_3N_4 (7 wt%) heterostructures at an excitation wavelength of 325 nm.

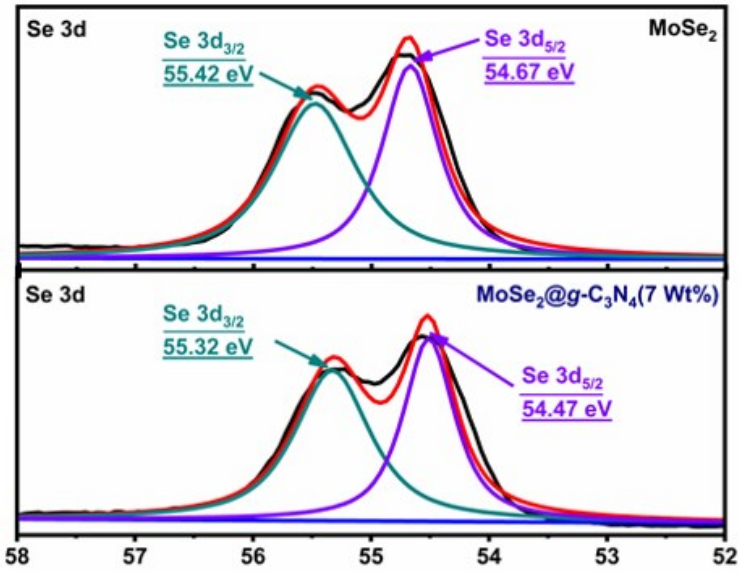

Figure S7: Se 3d spectra of $MoSe_2$ and $MoSe_2$@g-C_3N_4 hybrid (7 wt%).

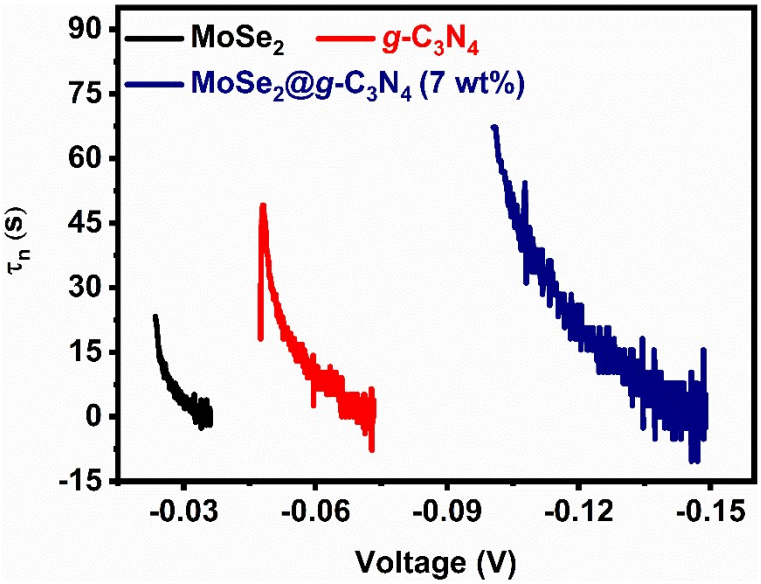

Figure S8: Average lifetimes of the photogenerated carriers (τ_n) obtained from the OCVD measurement for g-C_3N_4, $MoSe_2$ and $MoSe_2$@g-C_3N_4 (7 wt%) hybrid.

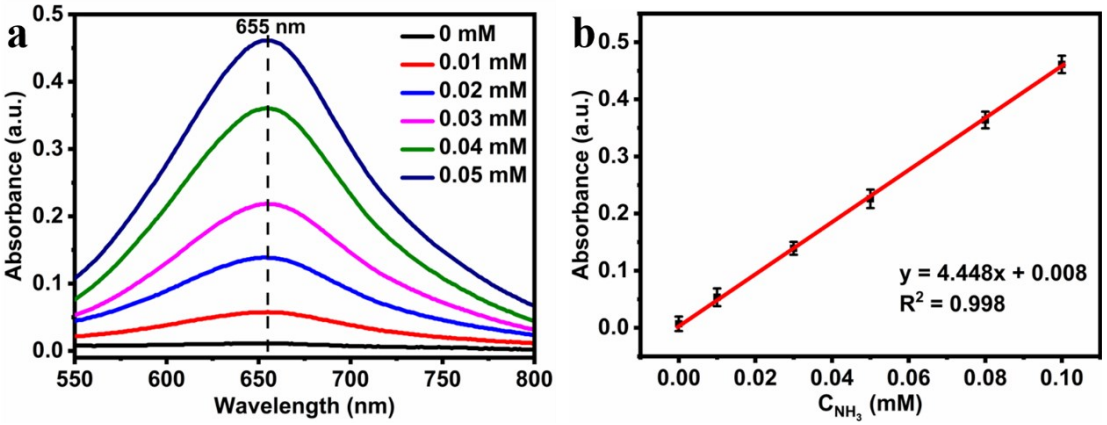

Figure S9: (a) UV–vis absorption spectra of indophenol assays with NH_4^+ ions in 0.1 M KOH electrolyte after incubated for 2 h at room temperature, (b) Calibration curve used for estimation of NH_3 by NH_4^+ ion concentration.

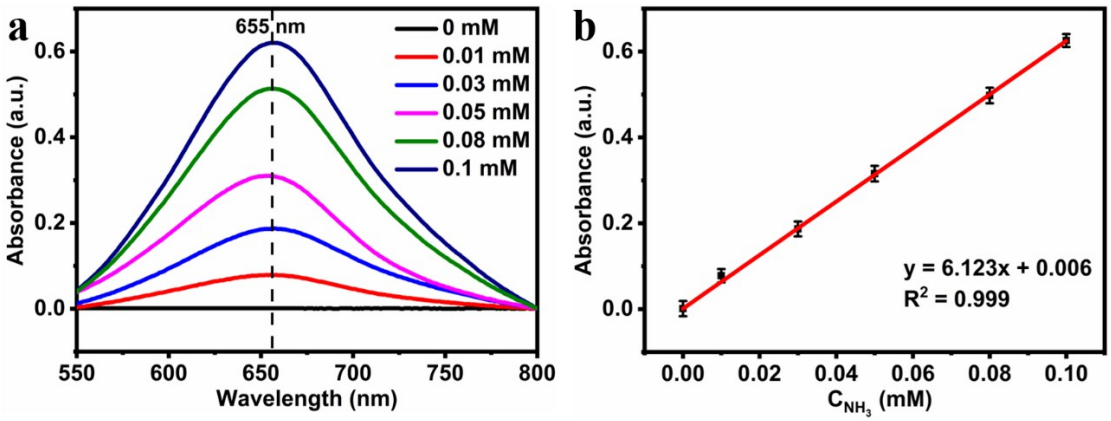

Figure S10: (a) UV–vis absorption spectra of indophenol assays with NH_4^+ ions in 0.05 M H_2SO_4 electrolyte after incubated for 2 h at room temperature, (b) Calibration curve used for estimation of NH_3 by NH_4^+ ion concentration.

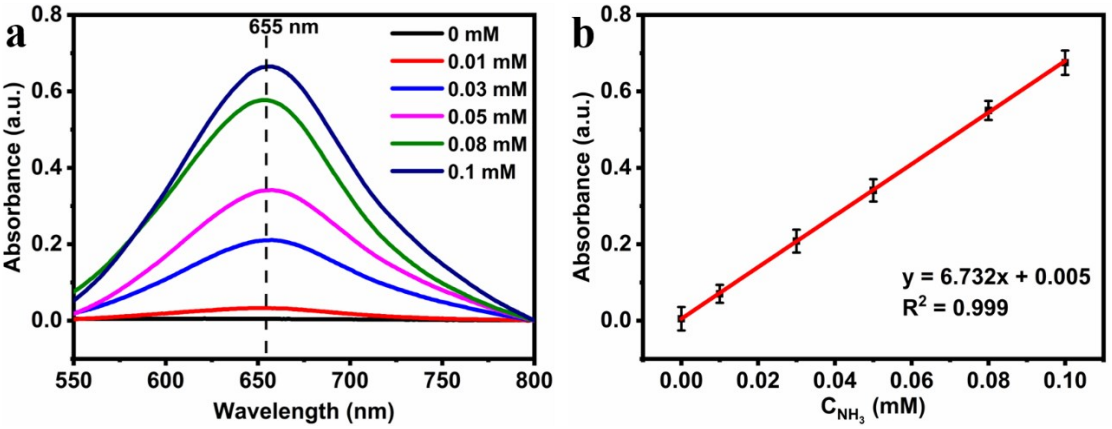

Figure S11: (a) UV–vis absorption spectra of indophenol assays with NH_4^+ ions in 0.1 M Na_2SO_4 electrolyte after incubated for 2 h at room temperature, (b) Calibration curve used for estimation of NH_3 by NH_4^+ ion concentration.

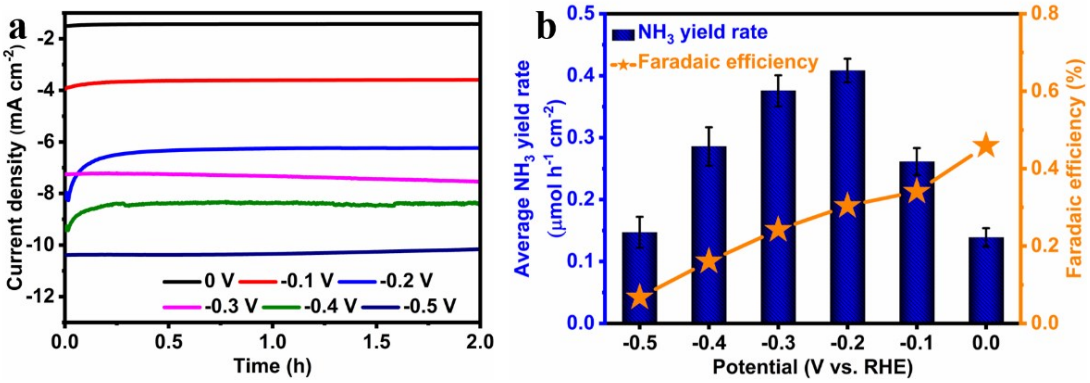

Figure S12：(a) Chronoamperometric results of electrocatalysis of N_2 by using $MoSe_2$ in 0.05 M H_2SO_4 electrolyte at potential ranging from 0 V to −0.5 V vs. RHE for 2 h without illumination, (b) Corresponding NH_3 yield rates and Faradaic efficiencies.

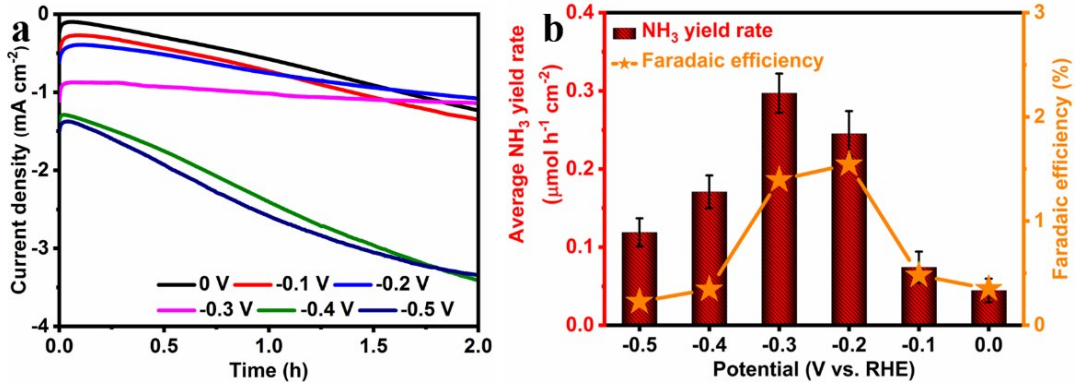

Figure S13: (a) Chronoamperometric results of electrocatalysis of N_2 by using $MoSe_2$ in 0.1 M Na_2SO_4 electrolyte at potential ranging from 0 V to −0.5 V vs. RHE for 2 h without illumination, (b) Corresponding NH_3 yield rates and Faradaic efficiencies.

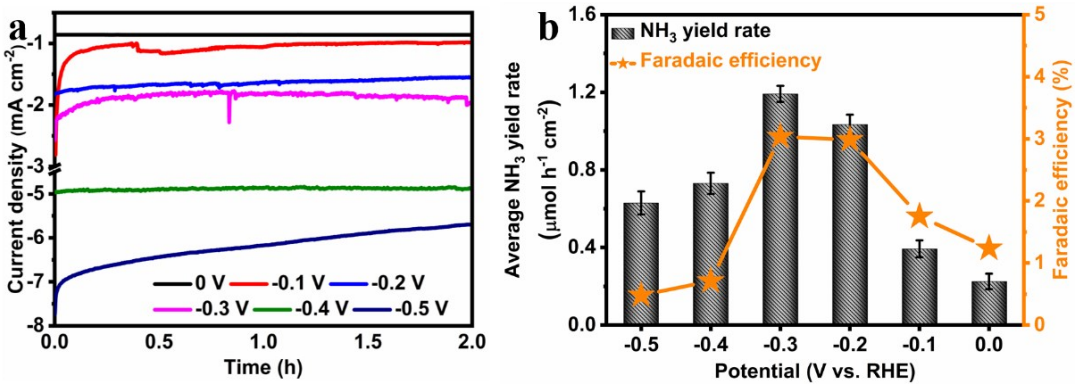

Figure S14: (a) Chronoamperometric results of electrocatalysis of N_2 by using $MoSe_2$ in 0.1 M KOH electrolyte at potential ranging from 0 V to −0.5 V vs. RHE for 2 h without illumination, (b) Corresponding NH_3 yield rates and Faradaic efficiencies.

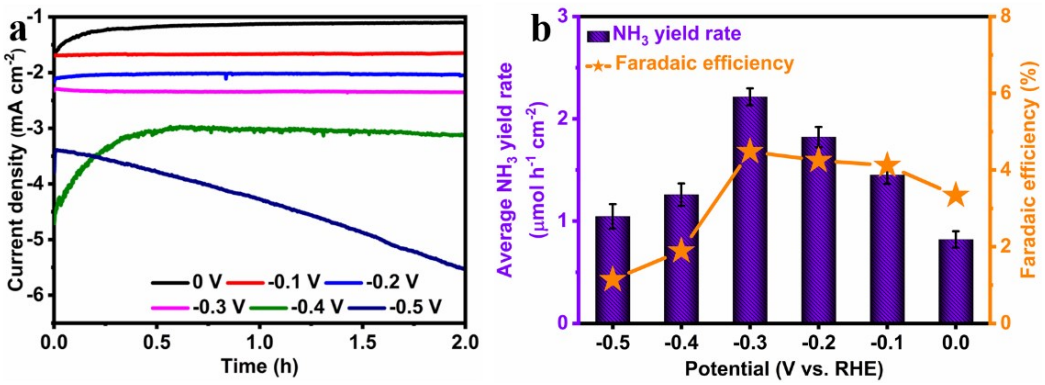

Figure S15: (a) Chronoamperometric results of photoelectrocatalysis of N_2 by using *g*-C_3N_4 in 0.1 M KOH electrolyte at potential ranging from 0 V to −0.5 V vs. RHE for 2 h under illumination, (b) Corresponding NH_3 yield rates and Faradaic efficiencies.

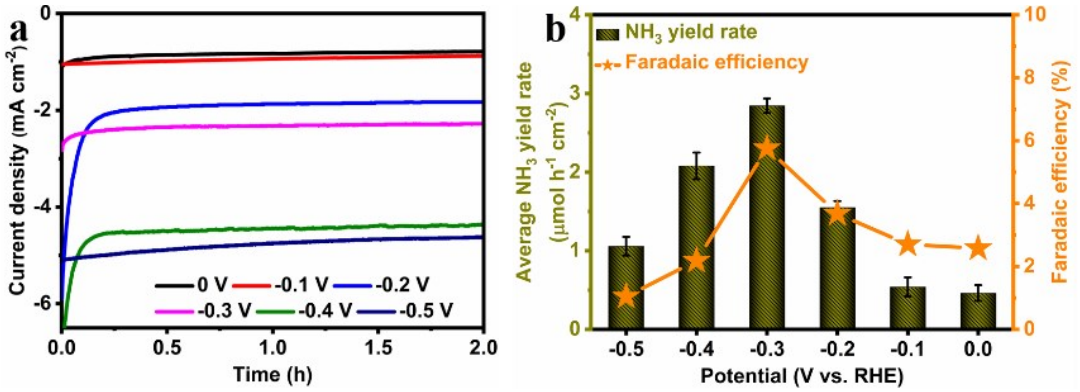

Figure S16: (a) Chronoamperometric results of photoelectrocatalysis of N_2 by using $MoSe_2$ in 0.1 M KOH electrolyte at potential ranging from 0 V to −0.5 V vs. RHE for 2 h under illumination, (b) Corresponding NH_3 yield rates and Faradaic efficiencies.

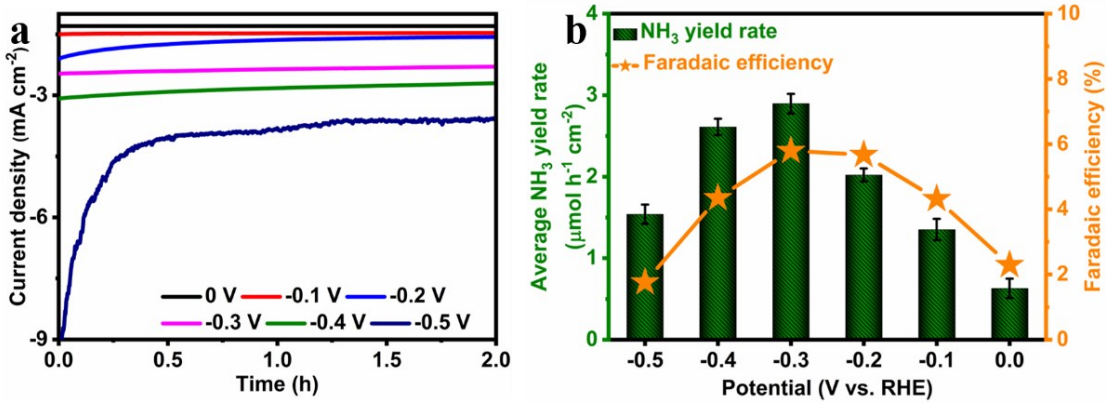

Figure S17: (a) Chronoamperometric results of photoelectrocatalysis of N_2 by using $MoSe_2$@g-C_3N_4 (1 wt%) in 0.1 M KOH electrolyte at potential ranging from 0 V to −0.5 V vs. RHE for 2 h under illumination, (b) Corresponding NH_3 yield rates and Faradaic efficiencies.

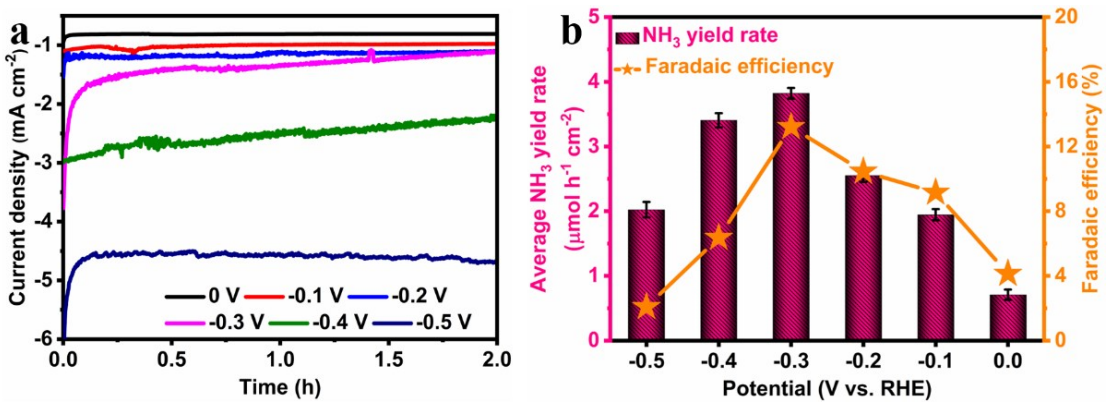

Figure S18: (a) Chronoamperometric results of photoelectrocatalysis of N_2 by using $MoSe_2$@*g*-C_3N_4 (3 wt%) in 0.1 M KOH electrolyte at potential ranging from 0 V to −0.5 V vs. RHE for 2 h under illumination, (b) Corresponding NH_3 yield rates and Faradaic efficiencies.

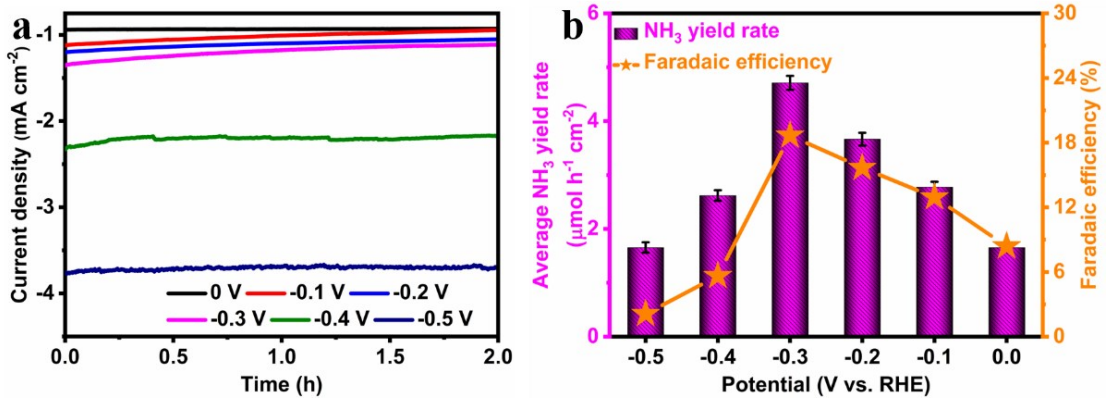

Figure S19: (a) Chronoamperometric results of photoelectrocatalysis of N_2 by using $MoSe_2$@*g*-C_3N_4 (5 wt%) in 0.1 M KOH electrolyte at potential ranging from 0 V to −0.5 V vs. RHE for 2 h under illumination, (b) Corresponding NH_3 yield rates and Faradaic efficiencies.

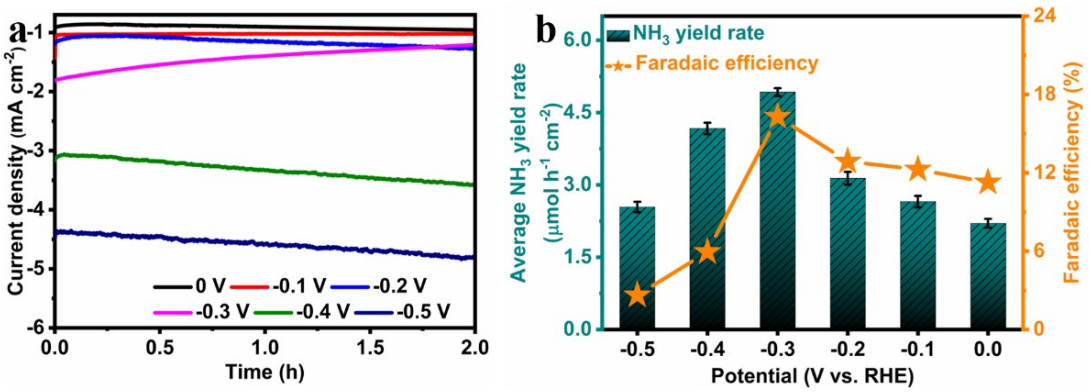

Figure S20: (a) Chronoamperometric results of photoelectrocatalysis of N_2 by using $MoSe_2$@*g*-C_3N_4 (9 wt%) in 0.1 M KOH electrolyte at potential ranging from 0 V to −0.5 V vs. RHE for 2 h under illumination, (b) Corresponding NH_3 yield rates and Faradaic efficiencies.

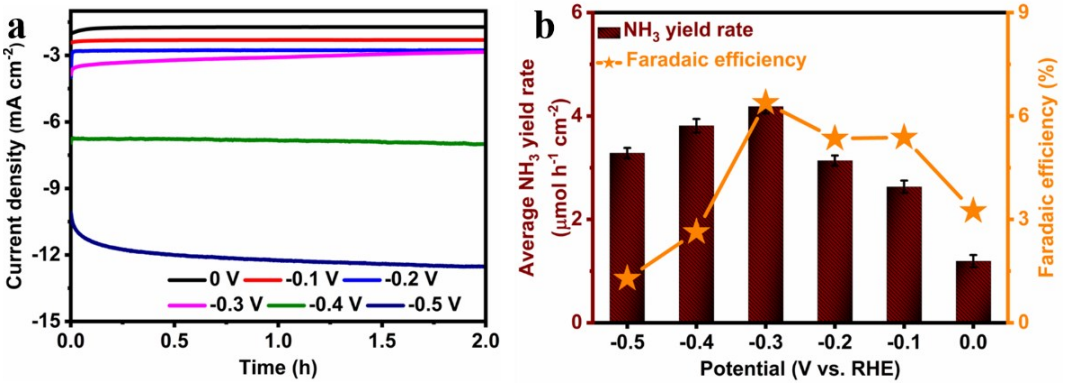

Figure S21: (a) Chronoamperometric results of photoelectrocatalysis of N_2 by using $MoSe_2$@*g*-C_3N_4 (11 wt%) in 0.1 M KOH electrolyte at potential ranging from 0 V to −0.5 V vs. RHE for 2h under illumination, (b) Corresponding NH_3 yield rates and Faradaic efficiencies.

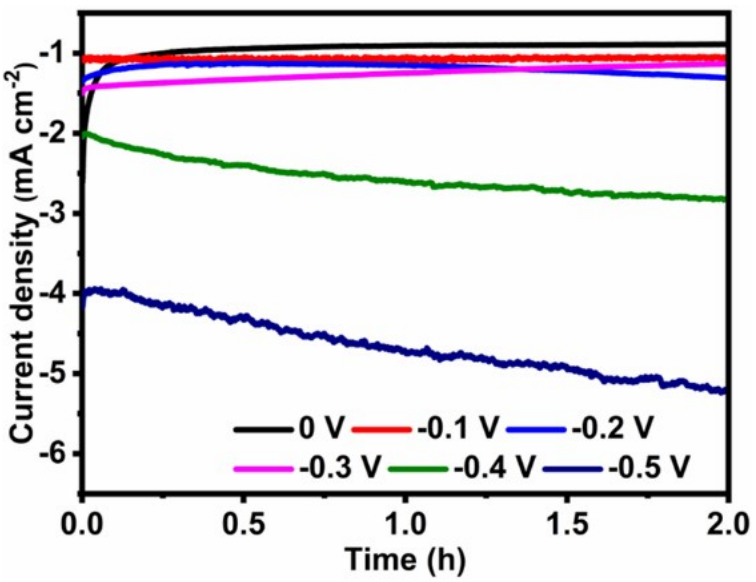

Figure S22: Chronoamperometric curves of $MoSe_2$@*g*-C_3N_4 (7 wt%) at different potentials under illumination.

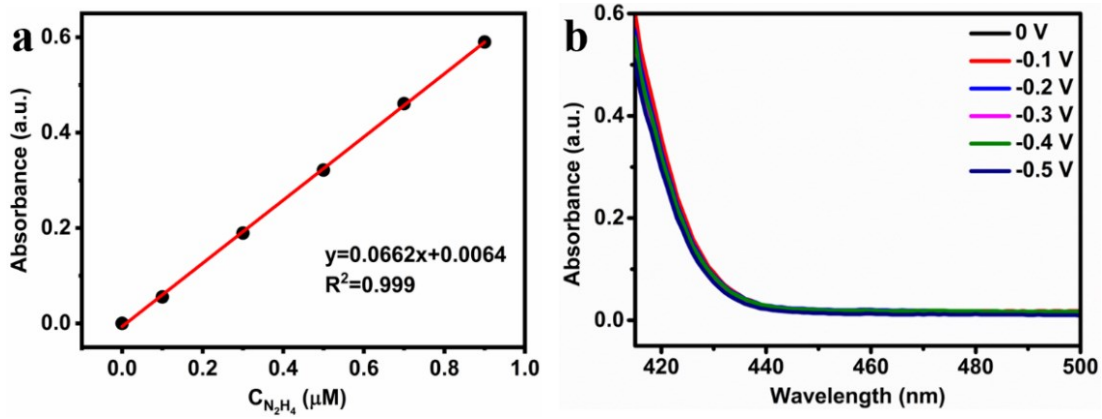

Figure S23: UV–vis absorption spectra of the electrolytes estimated by the method of Watt and Chrisp after PEC NRR at different potentials.

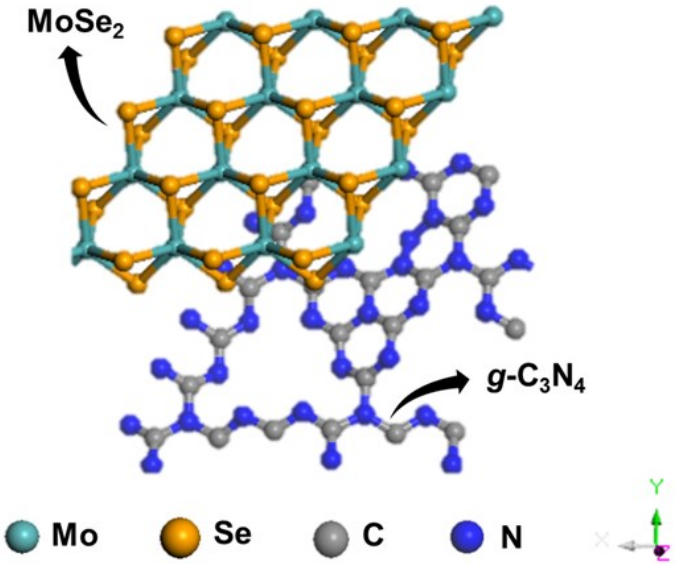

Figure S24: Structural model of $MoSe_2$@*g*-C_3N_4 heterojunctions.

Table S2: Formulation name, catalysis type, highest NH_3 yield rate and FE as well as electrolytes under ambient conditions. (Note: electrochemical; EC, photoelectrochemical; PEC).

Sr. No.	Formulation	Catalysis type	Electrolyte	NH_3 yield rate	V vs. RHE	FE	V vs. RHE
				μmol h^{-1} cm^{-1}	V	%	V
1	$MoSe_2$	EC	0.05 M H_2SO_4	0.4	−0.2	0.45	0
2	$MoSe_2$	EC	0.1 M Na_2SO_4	0.29	−0.3	1.54	−0.2
3	$MoSe_2$	EC	0.1 M KOH	1.19	−0.3	3.03	−0.3
4	*g*-C_3N_4	PEC	0.1 M KOH	2.21	−0.3	4.48	−0.3
5	$MoSe_2$	PEC	0.1 M KOH	2.84	−0.3	5.75	−0.3
6	$MoSe_2$@*g*-C_3N_4 (1 wt %)	PEC	0.1 M KOH	2.89	−0.3	5.79	−0.3
7	$MoSe_2$@*g*-C_3N_4 (3 wt %)	PEC	0.1 M KOH	3.82	−0.3	13.2	−0.3
8	$MoSe_2$@*g*-C_3N_4 (5 wt %)	PEC	0.1 M KOH	4.7	−0.3	18.7	−0.3
9	**$MoSe_2$@*g*-C_3N_4 (7 wt %)**	**PEC**	**0.1 M KOH**	**7.72**	**−0.3**	**28.9**	**−0.3**
10	$MoSe_2$@*g*-C_3N_4 (9 wt %)	PEC	0.1 M KOH	4.92	−0.3	16.2	−0.3
11	$MoSe_2$@*g*-C_3N_4 (11 wt %)	PEC	0.1 M KOH	4.18	−0.3	6.38	−0.3

Table S3: Summary of the representative reports on artificial electrochemical (EC) N_2 fixation under ambient conditions.

Catalyst system	**Electrolyte**	**NH_3 yield rate**	**FE (%)**	**Ref.**
$MoSe_2$@*g*-C_3N_4	**0.1 M KOH**	**7.72 μmol h^{-1} cm^{-2} or 2.14 nmol s^{-1} cm^{-2} or 131.47 μg h^{-1} cm^{-2} or 131.47 μg h^{-1} mg_{cat}^{-1}**	**28.9**	**This work**
1T@2H $MoSe_2$	0.1 M Na_2SO_4	19.91 μg h^{-1} mg_{cat}^{-1}	2.82	6
$MoSe_2$	0.1 M Na_2SO_4	11.2 μg h^{-1} mg_{cat}^{-1}	14.2	7
R-WO_3 NSs	0.1 M HCl	17.28 μg h^{-1} $mg_{cat.}^{-1}$	7.0	8
Boron nanosheet	0.1 M Na_2SO_4	13.22 μg h^{-1} $mg_{cat.}^{-1}$	4.04	9
AuCuB	0.1 M Na_2SO_4	13.2 μg h^{-1} $mg_{cat.}^{-1}$	12.78	10
MoN	0.1 M HCl	3×10^{-10} mol s^{-1} cm^{-2}	1.15	11
$Bi_4V_2O_{11}/CeO_2$	0.1 M HCl	23.21 μg h^{-1} $mg_{cat.}^{-1}$	10.16	12
Nb_2O_5 nanofiber	0.1 M HCl	43.6 μg h^{-1} $mg_{cat.}^{-1}$	9.26	13
Au flowers	0.1 M HCl	25.57 μg h^{-1} $mg_{cat.}^{-1}$	6.05	14
VO_2 hollow Microsphere	0.1 M Na_2SO_4	14.85 μg h^{-1} $mg_{cat.}^{-1}$	3.97	15
MnO	0.1 M Na_2SO_4	1.1×10^{-10} mol s^{-1} cm^{-2}	8.02	16
MoO_3	0.1 M HCl	29.43 μg h^{-1} $mg_{cat.}^{-1}$	1.9	17
S-doped carbon nanospheres	0.1 M Na_2SO_4	19.07 μg h^{-1} $mg_{cat.}^{-1}$	7.47	18
Rh NNs	0.1 M KOH	7.45 mg h^{-1} cm^{-2}	0.21	19
PdRu	0.1 M KOH	37.23 mg h^{-1} mg^{-1}	1.85	20
Ag nanosheet	0.1 M HCl	4.6×10^{-11} mol s^{-1} cm^{-2}	4.8	21
Cu Dendritic	0.1 M HCl	25.63 μg h^{-1} mg^{-1}	15.12	22
Bi Nanosheets	0.1 M Na_2SO_4	23.4 μg h^{-1} $mg_{cat.}^{-1}$	19.8	23
CoVP@NiFeV	0.05 M H_2SO_4	1.6 μmol h^{-1} cm^{-2}	13.8	24
Co-doped (NPC)	0.1 M HCl	0.97 μg h^{-1} mg^{-1}	4.2	25
$Pd_{0.2}Cu_{0.8}$/rGO	0.1 M KOH	2.80 μg h^{-1} mg^{-1}	0.6	26
Au-CNT	0.1 M HCl	57.7 μg h^{-1} cm^{-2}	11.97	27
Carbon nanotubes	0.1 M $LiClO_4$	32.33 μg h^{-1} mg^{-1}	12.50	28
Mn_3O_4@rGO	0.1 M Na_2SO_4	17.4 μg h^{-1} mg^{-1}	3.52	29
Pt	2 M KOH	0.19 μg h^{-1} mg^{-1}	0.01	30
Re_2MnS_6	0.1 M Na_2SO_4	3.78 μg h^{-1} mg_{cat}^{-1}	17.42	31
NbO_2	0.05 M H_2SO_4	11.6 μg h^{-1} $mg_{cat.}^{-1}$	32	32

Table S4: Summary of the representative reports on artificial photochemical (PC) N_2 fixation under ambient conditions.

Catalyst system	Electrolyte	NH_3 yield rate	FE (%)	Ref.
$MoSe_2$@g-C_3N_4	**0.1 M KOH**	**7.72 μmol h^{-1} cm^{-2}**	**28.9**	**This work**
FeAl@3D Graphene	Water	25.3 μmol h^{-1} g^{-1}	–	[33]
Bi_5O_7I nanosheets	0.1 M Na_2SO_4	111.5 μmol h^{-1} g^{-1}	5.1	[34]
BiO quantum dots	Water	1226 mmol h^{-1} g^{-1}	–	[35]
Bi_5O_7Br nanotubes	Water	1380 mmol h^{-1} g^{-1}	2.3	[36]
Bi_2MoO_6	Water and	1300 μmol h^{-1} g^{-1}	0.73	[37]
BiOCl	0.01 M $NaClO_4$	4.62 μmol h^{-1} g^{-1}	4.3	[38]
Mo-doped $W_{18}O_{49}$	0.5 M Na_2SO_4	195.5 μmol h^{-1} g^{-1}	0.33	[39]
S, N co-doped $(BiO)_2CO_3$	CH_3CN and water	38.2 μmol h^{-1} g^{-1}	0.006	[40]
BiOBr nanosheets	0.5 M Na_2SO_4	10.42 mmol h^{-1} g^{-1}	0.23	[41]
Ultrathin MoS_2	Ethanol and water	325 μmol h^{-1} g^{-1}	–	[42]

References

1. J. Bisquert, A. Zaban, M. Greenshtein and I. Mora-Seró, *Journal of the American Chemical Society*, 2004, **126**, 13550-13559.
2. G. Kresse and D. Joubert, *Physical review b*, 1999, **59**, 1758.
3. J. P. Perdew, K. Burke and M. Ernzerhof, *Physical Review Letters*, 1996, **77**, 3865.
4. S. Grimme, J. Antony, S. Ehrlich and H. Krieg, *The Journal of chemical physics*, 2010, **132**, 154104.
5. X. Yu, P. Han, Z. Wei, L. Huang, Z. Gu, S. Peng, J. Ma and G. Zheng, *Joule*, 2018, **2**, 1610-1622.
6. Z. Wu, R. Zhang, H. Fei, R. Liu, D. Wang and X. Liu, *Applied Surface Science*, 2020, **532**, 147372.
7. L. Yang, H. Wang, X. Wang, W. Luo, C. Wu, C.-a. Wang and C. Xu, *Inorganic Chemistry*, 2020, DOI: 10.1021/acs.inorgchem.0c02058.
8. W. Kong, R. Zhang, X. Zhang, L. Ji, G. Yu, T. Wang, Y. Luo, X. Shi, Y. Xu and X. Sun, *Nanoscale*, 2019, **11**, 19274-19277.
9. X. Zhang, T. Wu, H. Wang, R. Zhao, H. Chen, T. Wang, P. Wei, Y. Luo, Y. Zhang and X. Sun, *ACS Catalysis*, 2019, **9**, 4609-4615.
10. Z. Wang, J. Niu, Y. Xu, L. Wang, H. Wang and H. Liu, *ACS Sustainable Chemistry & Engineering*, 2020, **8**, 12588-12594.
11. L. Zhang, X. Ji, X. Ren, Y. Ma, X. Shi, Z. Tian, A. M. Asiri, L. Chen, B. Tang and X. Sun, *Advanced Materials*, 2018, **30**, 1800191.
12. C. Lv, C. Yan, G. Chen, Y. Ding, J. Sun, Y. Zhou and G. Yu, *Angewandte Chemie International Edition*, 2018, **57**, 6073-6076.
13. J. Han, Z. Liu, Y. Ma, G. Cui, F. Xie, F. Wang, Y. Wu, S. Gao, Y. Xu and X. Sun, *Nano Energy*, 2018, **52**, 264-270.
14. Z. Wang, Y. Li, H. Yu, Y. Xu, H. Xue, X. Li, H. Wang and L. Wang, *ChemSusChem*, 2018, **11**, 3480-3485.
15. R. Zhang, H. Guo, L. Yang, Y. Wang, Z. Niu, H. Huang, H. Chen, L. Xia, T. Li and X. Shi, *ChemElectroChem*, 2019, **6**, 1014-1018.
16. Z. Wang, F. Gong, L. Zhang, R. Wang, L. Ji, Q. Liu, Y. Luo, H. Guo, Y. Li and P. Gao, *Advanced Science*, 2019, **6**, 1801182.
17. J. Han, X. Ji, X. Ren, G. Cui, L. Li, F. Xie, H. Wang, B. Li and X. Sun, *Journal of Materials Chemistry A*, 2018, **6**, 12974-12977.
18. L. Xia, X. Wu, Y. Wang, Z. Niu, Q. Liu, T. Li, X. Shi, A. M. Asiri and X. Sun, *Small Methods*, 2019, **3**, 1800251.
19. H.-M. Liu, S.-H. Han, Y. Zhao, Y.-Y. Zhu, X.-L. Tian, J.-H. Zeng, J.-X. Jiang, B. Y. Xia and Y. Chen, *Journal of Materials Chemistry A*, 2018, **6**, 3211-3217.
20. H. Wang, Y. Li, C. Li, K. Deng, Z. Wang, Y. Xu, X. Li, H. Xue and L. Wang, *Journal of Materials Chemistry A*, 2019, **7**, 801-805.
21. H. Huang, L. Xia, X. Shi, A. M. Asiri and X. Sun, *Chemical Communications*, 2018, **54**, 11427-11430.
22. C. Li, S. Mou, X. Zhu, F. Wang, Y. Wang, Y. Qiao, X. Shi, Y. Luo, B. Zheng, Q. Li and X. Sun, *Chemical Communications*, 2019, **55**, 14474-14477.
23. J. Wang, Y. Ren, M. Chen, G. Cao, Z. Chen and P. Wang, *Journal of Alloys and Compounds*, 2020, 154668.

24. M. Arif, G. Yasin, L. Luo, W. Ye, M. A. Mushtaq, X. Fang, X. Xiang, S. Ji and D. Yan, *Applied Catalysis B: Environmental*, 2020, **265**, 118559.
25. P. Song, H. Wang, L. Kang, B. Ran, H. Song and R. Wang, *Chemical Communications*, 2019, **55**, 687-690.
26. M. M. Shi, D. Bao, S. J. Li, B. R. Wulan, J. M. Yan and Q. Jiang, *Advanced Energy Materials*, 2018, **8**, 1800124.
27. X. Zhao, Z. Yang, A. V. Kuklin, G. V. Baryshnikov, H. Agren, X. Zhou and H. Zhang, *ACS Applied Materials & Interfaces*, 2020, DOI: 10.1021/acsami.0c11487.
28. J. Zhao, B. Wang, Q. Zhou, H. Wang, X. Li, H. Chen, Q. Wei, D. Wu, Y. Luo and J. You, *Chemical Communications*, 2019, **55**, 4997-5000.
29. H. Huang, F. Gong, Y. Wang, H. Wang, X. Wu, W. Lu, R. Zhao, H. Chen, X. Shi, A. M. Asiri, T. Li, Q. Liu and X. Sun, *Nano Research*, 2019, **12**, 1093-1098.
30. B. L. Sheets and G. G. Botte, *Chemical Communications*, 2018, **54**, 4250-4253.
31. Y. Fu, T. Li, G. Zhou, J. Guo, Y. Ao, Y. Hu, J. Shen, L. Liu and X. Wu, *Nano Letters*, 2020, **20**, 4960-4967.
32. L. Huang, J. Wu, P. Han, A. M. Al‐Enizi, T. M. Almutairi, L. Zhang and G. Zheng, *Small Methods*, 2019, **3**, 1800386.
33. Y. Lu, Y. Yang, T. Zhang, Z. Ge, H. Chang, P. Xiao, Y. Xie, L. Hua, Q. Li and H. Li, *ACS nano*, 2016, **10**, 10507-10515.
34. Y. Bai, L. Ye, T. Chen, L. Wang, X. Shi, X. Zhang and D. Chen, *ACS applied materials & interfaces*, 2016, **8**, 27661-27668.
35. S. Sun, Q. An, W. Wang, L. Zhang, J. Liu and W. A. Goddard III, *Journal of Materials Chemistry A*, 2017, **5**, 201-209.
36. S. Wang, X. Hai, X. Ding, K. Chang, Y. Xiang, X. Meng, Z. Yang, H. Chen and J. Ye, *Advanced Materials*, 2017, **29**, 1701774.
37. Y. Hao, X. Dong, S. Zhai, H. Ma, X. Wang and X. Zhang, *Chemistry–A European Journal*, 2016, **22**, 18722-18728.
38. H. Li, J. Shang, J. Shi, K. Zhao and L. Zhang, *Nanoscale*, 2016, **8**, 1986-1993.
39. N. Zhang, A. Jalil, D. Wu, S. Chen, Y. Liu, C. Gao, W. Ye, Z. Qi, H. Ju and C. Wang, *Journal of the American Chemical Society*, 2018, **140**, 9434-9443.
40. P. Ding, J. Di, X. Chen, M. Ji, K. Gu, S. Yin, G. Liu, F. Zhang, J. Xia and H. Li, *ACS Sustainable Chemistry & Engineering*, 2018, **6**, 10229-10240.
41. H. Li, J. Shang, Z. Ai and L. Zhang, *Journal of the American Chemical Society*, 2015, **137**, 6393-6399.
42. S. Sun, X. Li, W. Wang, L. Zhang and X. Sun, *Applied Catalysis B: Environmental*, 2017, **200**, 323-329.